

Contactless Shape Manipulation of Thin Substrates Using Air Bearing Table

Theresa M. Spaan-Burke¹, Teunis van Dam¹, Peter Overschie¹, Henny A.M. Spaan¹
¹IBS Precision Engineering,
Eindhoven, Netherlands

INTRODUCTION

Externally pressurized aerostatic bearings (from now on referred to as air bearings) are commonly used for conveying large area, thin substrates such as glass sheets [2], [3]. Pressurized air is provided through either orifices or a porous restrictor, establishing an air cushion on which the substrate floats. Regions of sub-atmospheric pressure ('vacuum holes or grooves') can be added to reduce the levitation height and improve the out-of-plane stiffness [3]. In addition, systems have been developed in which the substrate is not only levitated but also actuated in three planar directions, using viscous shear forces controlled by air jets or pressure differentials in the air gap [4]-[6]. A recent survey on this type of mechanisms is found in [7].

It is known that the pressure differentials below the substrate carried by an air bearing table influence the out-of-plane deformation. In theory, individual control of the pressure levels in separate regions of such an air table would allow a degree of control over this deformation. In this paper the feasibility of this concept is investigated. An air table is proposed with a number of separate air bearing regions and sub-atmospheric pressure regions. The pressure in the sub-atmospheric regions is controlled to bend the substrate into pre-defined shapes.

APPROACH

To prove the feasibility of the proposed technology, off-the-shelf Precision Air Bars (New Way Air Bearings®) were selected. Commercially available air bars were chosen over a custom design in order to reduce cost and lead time and because the stable behavior of these products is proven in Flat Panel Display applications. The air bars consist of a 2x8 array of rectangular porous air bearing sections, each containing a single 'vacuum hole' in its center. Here the term 'vacuum' is used to indicate a pressure that is sub-atmospheric. Normally the vacuum holes lead to a single chamber connected to an exhaust pump. For this situation

the air bars were modified to allow individual control of the vacuum pressures.

A \varnothing 150 mm circular reflective substrate was chosen as a sample substrate. The substrate deformation was captured using a Fizeau interferometer with \varnothing 150 mm field of view. The geometry of the air bars and circular substrate is shown schematically in Figure 1. Two air bars are placed next to each other and the substrate is placed onto the resulting air table such that it overlaps with twelve of the vacuum holes. The remaining vacuum holes (20 in total) are not used. Only the twelve porous air bearing segments corresponding with the numbered holes are used; the remaining air bearing surface being sealed including those covered partly by the substrate. In this way, the air flowing out of these segments was prevented from forcing the edge of the substrate upwards without compensation of a vacuum hole. Figure 2 shows a schematic cross-section view of a single bearing segment and vacuum hole.

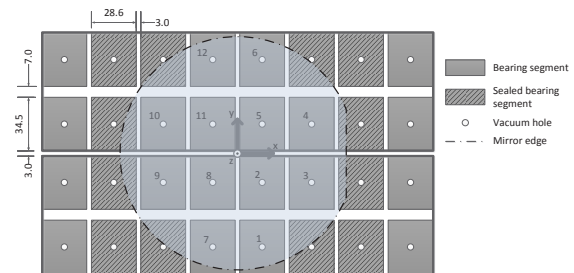


Figure 1. Layout of circular substrate on air table (top view) with definition of hole numbering and (x,y,z) coordinate system. Dimensions in mm.

A Finite Element simulation model was built with which the deformation of the substrate is predicted as a function of applied pressure levels. The ability to deform the substrate into shapes of different form and complexity is demonstrated by selecting a set of target forms, described by Zernike polynomials. The pressure differential patterns such that the resulting

substrate shapes approach these targets as close as possible were defined through this model.

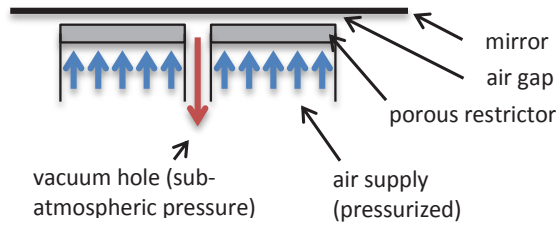


Figure 2 Schematic cross-section of single bearing segment and substrate (side view). The pressure differential between the porous air bearing region and the vacuum hole causes the thin substrate to deform.

An experimental setup was constructed to validate the outcome of the simulations. Vacuum pressure levels were manually manipulated using needle valves and a high-accuracy pressure meter. The resulting shape of the substrate was measured with a Fizeau interferometer. In comparing the measured and simulated substrate shape at identical pressure differential levels, the simulation model is validated.

In the simulation model, the initial deformation of the substrate could not be taken into account. To allow comparison between simulation and experimental results, only 'differential' deformed shapes are therefore compared. Both in the simulations and in the experiments a starting point is found where the pressure levels are optimized for a flat substrate, called the 'flat substrate reference'. In all the experiments where the substrate is forced into a certain shape by defined pressure differentials, the flat wafer reference shape is subtracted from the actual shape.

SIMULATION MODEL AND RESULTS

Nomenclature	
h	local air film thickness (m)
H	thickness of porous restrictor (m)
L	characteristic bearing length (m)
p	pressure in air film (Pa)
p_{amb}	ambient pressure (Pa)
p_{in}	supply pressure (Pa)
R_s	specific gas constant of air (J/kgK)
T	temperature (K)
κ	permeability of porous restrictor material (m ²)

Λ	dimensionless bearing number = $12\kappa L^2/h^3H$
μ	dynamic viscosity of air (Pa·s)

To predict the behavior of the substrate floating on the air table a Finite Element model was created in COMSOL Multiphysics®. The model consists of a structural domain, solving for the displacement and deformation of the substrate, and a fluid domain, solving for the pressure in the air film below the substrate. The physical domains are coupled in two directions: the pressure from the fluid domain acts as a distributed load on the structure, while the deformation of the structure defines the height of the air gap in the fluid domain.

Calculation methods to solve the pressure in the air film for porous air bearings consist of a combination of the compressible Reynold's equation with a source flow term as described in literature [7],[8]. In [8], several methods are compared with each other and with experimental data for simple rectangular and circular bearing geometries. A 'no slip' condition in Reynold's equation is compared with various slip models and experimental data over a range of prescribed gap heights. Based on the results of this study and the (partly estimated) dimensions and conditions in this case, using the assumptions of no slip and 1D source flow is justified and will likely not cause more than 1% difference on the outcome of the calculations. The resulting equation describing the pressure in the air film is then given by:

$$\nabla \left(\frac{h^3}{12\mu R_s T} p \nabla p \right) = \frac{\kappa}{2H\mu R_s T} (p_{in}^2 - p^2) \quad (1)$$

The combined model is solved for the geometry as presented in Figure 1 using the following conditions: $H = 4.5$ mm, $p_{in} = 5.1$ bar absolute, $R_s = 287$ J/kgK, $T = 20^\circ\text{C}$, $\mu = 1.81\text{e-}5$ Pa·s. The value for the permeability κ was determined empirically by measuring the mass flow through an air bar at a fixed pressure differential. In the grooves between the air bearing segments, ambient pressure is assumed: $p_{amb} = 1$ atm (1.013 bar).

For the substrate, it is assumed that the material properties and thickness are uniform and the substrate is initially flat and free of initial stresses. For the air bearing, it is assumed that the bearing surface is flat and the effective permeability and supply pressure are uniform over the entire surface of all twelve segments.

The calculation time to obtain the substrate shape for a single condition is approximately ten seconds.

Definition of Target Shapes

A set of Zernike polynomials is chosen as target shapes for controlled deformation of the substrate. The use of Zernike polynomials has the following advantages:

- The clear mathematical description of the shapes is convenient for comparison with the simulation outcome and experimental results
- The Zernike shapes are similar to the mechanical mode shapes of a free circular plate
- The Zernike shapes are orthogonal, which is useful for combining different shapes

Number	Image	Description
1		Piston
2,3		Tilt
4		Defocus
5,6		Astigmatism
7,8		Coma
7',8'		Coma, tilt corrected
9		2 nd order spherical aberration
10,11		Trefoil

Table 1. Definition of Zernike 1-11. Zernike 4-8 and 10 are used as target shapes. On Zernike 7 and 8, a tilt correction is applied.

The first eleven Zernike shapes, according to the numbering used in [9], are listed in Table 1. Zernike 4-8 and 10 are chosen as target shapes. Zernike 1-3 are not taken into account since they are only rigid body motions and not deformations of the surface, and Zernike 9 and 12 and higher are cannot be realized with the limited number of control points in the chosen bearing configuration. Zernike 7 and 8 are corrected for tilt as shown in the table.

The pressure patterns optimized for each of the target shapes are shown in Table 2. The differential pressure patterns are always chosen such that the average is zero, keeping the average applied pressure at 100 mbar below ambient.

hole #	1	2	3	4	5	6	7	8	9	10	11	12	avg
Z4	25	-49	24	24	-49	25	25	-49	24	24	-49	25	0
Z5	-71	15	56	56	15	-71	-72	15	56	56	15	-72	0
Z6	-31	-14	-44	38	23	28	28	23	38	-44	-14	-31	0
Z7	2	-56	-20	-20	-55	2	5	44	24	24	44	5	0
Z8	14	45	13	-7	-55	-10	14	45	13	-7	-55	-10	0
Z10	-45	-5	26	26	-5	-45	42	13	-30	-30	13	42	0

Table 2. Differential pressure patterns for each Zernike setpoints (mbar).

The resulting calculated differential substrate shapes are shown in Figure 3 and the average fly height and P-V amplitude of these shapes are listed in Table 3.

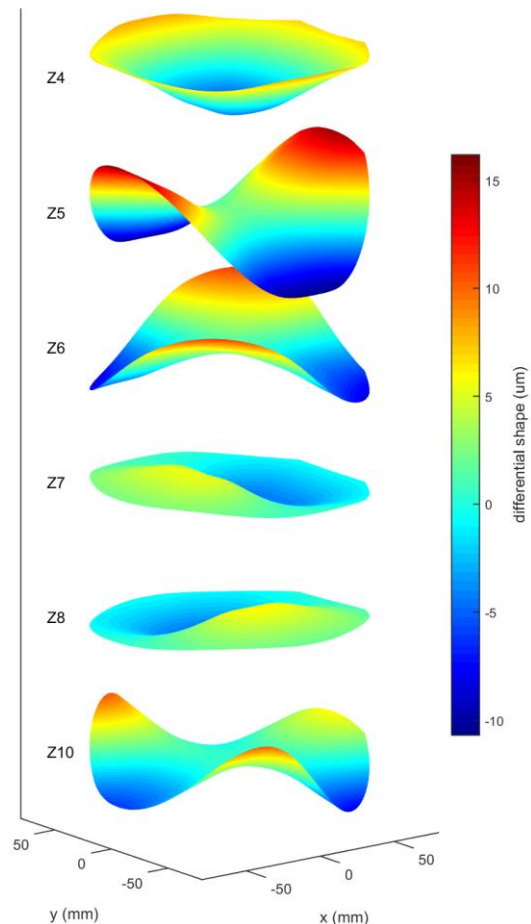


Figure 3. Calculated differential substrate shapes in μm using pressure patterns optimized for target Zernike shapes Z4-Z8 and Z10 (Table 2). All shapes scaled with the same ratio in z-direction

Shape	Average fly height (μm)	Amplitude of differential shape ($\mu\text{m P-V}$)	RMS deviation from Zernike (μm)
Z4	43.0	13.8	0.79
Z5	43.7	26.8	0.72
Z6	42.0	19.5	0.62
Z7	41.8	9.6	0.74
Z8	41.7	10.6	0.76
Z10	41.6	18.2	0.99

Table 3. Average fly height, P-V amplitude of differential shape and RMS deviation from Zernike for each of the calculated substrate shapes.

For each of the results, the best-fit corresponding Zernike shape is subtracted to get the 'shape deviation'. The RMS values of the shape deviation are also listed in Table 3.

Combining and Scaling Target Shapes

Simulations were conducted to demonstrate the possibility of combining and scaling the realized shapes. Although the equations are not linear, it might still be possible to achieve linear combinations of the individual target shapes using linear combinations of the corresponding pressure patterns. Therefore combined target shape '(Z4+Z6)/2' and a reduced target shape 'Z6/2' are defined. For the '(Z4+Z6)/2' target, the differential pressure level is given by the average of that for Z4 and Z6. For the 'Z6/2' target, the differential pressure level for Z6 is scaled down with a factor two.

The calculated differential substrate shape for (Z4+Z6)/2 and Z6/2 are compared with the 'expected' shapes – the corresponding combination and scaling of the previously calculated shapes for the individual Z4 and Z6 conditions. The results for (Z4+Z6)/2 are shown in Figure 4. The P-V amplitude of the expected and calculated shapes, and the RMS deviation between the expected and calculated shapes are given in Table 4.

Although the equations describing the relation between pressure and substrate deformation are non-linear, the system behaves approximately linearly in this region: when combining and scaling the pressure patterns of two selected target shapes, the resulting substrate shapes match fairly well with the shapes that would be

expected when combining or scaling the original shapes.

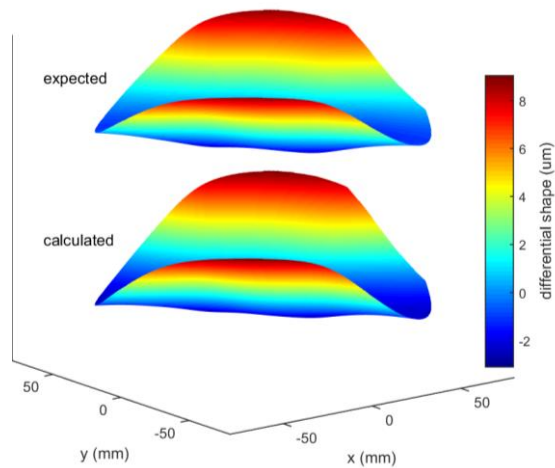


Figure 4. Expected and calculated differential substrate shape for combination of Z4 and Z6 '(Z4+Z6)/2'.

Shape	Amplitude expected diff. shape ($\mu\text{m P-V}$)	Amplitude calculated diff. shape ($\mu\text{m P-V}$)	RMS deviation (μm)
Z6/2	9.9	9.6	0.14
(Z4+Z6)/2	11.7	12.2	0.33

Table 4. Amplitude of expected and calculated shape and RMS deviation for combined and scaled target shapes.

EXPERIMENTAL SETUP AND PROCEDURE

The experimental setup is shown in Figure 5. The air bars are fixed to the bottom side of an interface plate. The specified flatness for each air bar is $< 2 \mu\text{m}$ over the entire bearing surface (16 segments) and the air bars are aligned with respect to each other such that the flatness of the combined surface is $< 3 \mu\text{m}$. The hole in the interface plate indicates the location where the substrate (not shown) is placed onto the air table. The in-plane position and orientation of the substrate are fixed by four end-stops leaving a clearance of 0.1-0.2 mm to all sides. The center of the substrate is aligned with the center of the air table within $\pm 1.5 \text{ mm}$ in x and y direction. The orientation of the substrate relative to the air table is within $\pm 1.0^\circ$ of the orientation shown in Figure 1.

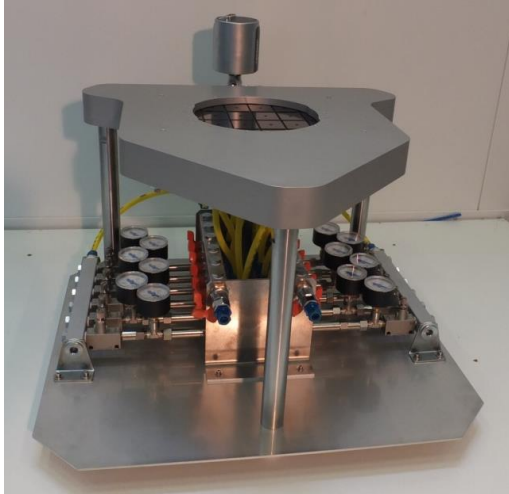


Figure 5. Experimental setup.

All porous bearing segments are connected to a single air supply line. The twelve vacuum holes are connected to twelve separate vacuum channels each with a needle valve for manipulating the pressure levels and a pressure gauge for rough pressure indication (see Figure 5). A set of manifolds connects the vacuum channels to a absolute pressure meter with a range of 0-1000 Torr (0-1.333 bar absolute) and an absolute accuracy of ± 2.5 mbar. Each vacuum channel can be connected to the pressure meter by means of a pneumatic valve.

The twelve vacuum pressure levels are manually set to the desired values by switching the vacuum channels one by one onto the pressure meter and manipulating the corresponding needle valve until the indicated value corresponds to the desired value within 1 mbar. Once all pressures are set, the interferometer image is taken. The image is converted into a height plot by μ Shape™ software.

EXPERIMENTAL RESULTS

The differential pressure patterns as used in the simulations for realizing the target shapes (Table 2) are applied. The shape of the substrate is measured for each of the conditions. The results are presented in Figure 6.

In Figure 7 cross sections are shown of the shapes, along with the shapes as predicted with the simulation model. The amplitude of the measured differential shapes and RMS deviation from the simulation results are shown in Table 5.

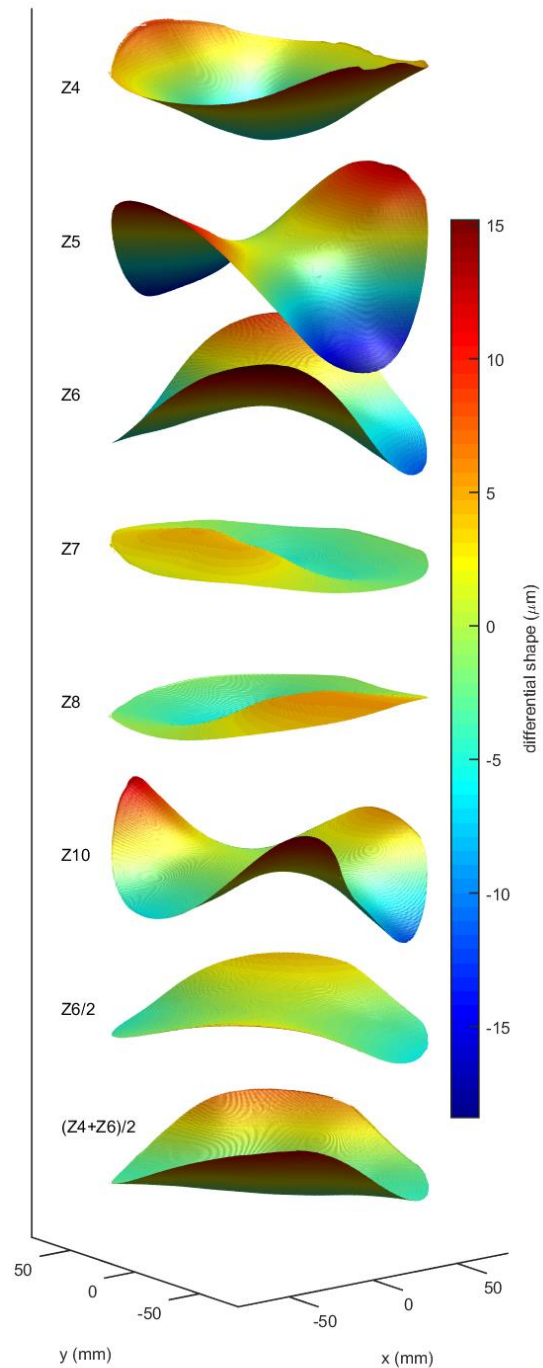


Figure 6. Measured differential substrate shapes for each of the Zernike target shape pressure patterns.

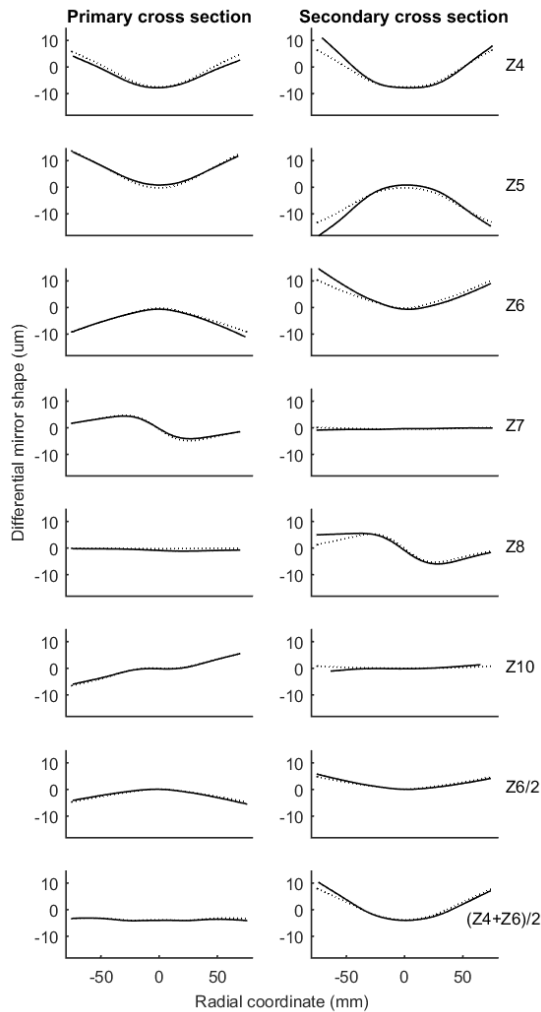


Figure 7. Cross sections of the differential substrate shape: experiments (solid line); simulations (dotted line). Primary -X axis; secondary-Y axis.

Shape	RMS deviation (µm)	Shape	RMS deviation (µm)
Z4	1.6	Z8	1.0
Z5	1.1	Z10	1.0
Z6	1.4	Z6/2	0.5
Z7	0.5	(Z4+Z6)/2	0.8

Table 5. Numerical results for the experiments.

DISCUSSION

Figure 7 and Table 5 show overall an excellent correlation between the simulated Zernike shapes and those measured. In the cross sections in Figure 7, it can be seen that a deviation between the calculated and measured shape occurs locally in most of the shapes, each time located in the south (negative y) or southwest (negative x, negative y) corner of the

substrate as shown in Figure 6. Here the deviation is significantly larger than over the rest of the area. In the Z7 and Z10 shapes this effect is less clearly visible. For the Z7 and Z8 shape – where the peaks of the deformed shape are not on the edge of the substrate – the P-V value matches much better with the simulations than for the other shapes, where the peaks are on the edge. Based on these observations, the conclusion can be drawn that the differences between the measured and simulated shapes are dominated by effects at the edge of the substrate and especially the specific local effect at the south/southwest corner of the substrate. This latter effect may be caused by an artefact (local weakness) in the substrate; as in all cases it bends more extremely than predicted in this corner, regardless whether it bends upwards or downwards. This could be confirmed by 90° rotation of the substrate on the air table. Limited access to the interferometer precluded such a test, which will be part of future testing.

REFERENCES

- [1] Saathof R, Schutten GJM, Spronck JW, Munnig Schmidt RH, Design and characterization of an active substrate for EUV-lithography, Precision Engineering 41 (2015) 102-110
- [2] Hoetzle M, Dunifon T, and Rozevink L, Glass transportation system. U.S. Patent 6,505,483, 2003.
- [3] Devitt AJ, Non-contact porous air bearing and glass flattening device. U.S. Patent 7,908,885, 2011.
- [4] van Rij J *et al.* Planar wafer transport and positioning on an air film using a viscous traction principle. Tribology International, 42:1542–1549, 2009.
- [5] Wesselingh J, Contactless Positioning using an Active Air Fil, PhD Thesis, ISBN978-90-9026437-0.
- [6] Delettre A, Guillaume JL and Le Fort-Piat. "A new contactless conveyor system for handling clean and delicate products using induced air flows. IROS2010 RSJ International Conference IEEE, 2010.
- [7] Laurent, GJ and Moon H, "A survey of non-prehensile pneumatic manipulation surfaces: principles, models and control." Intelligent Service Robotics 8.3 (2015): 151-163.
- [8] Witelski T, Schwendeman D, and Evans. "Analysis of Pressurized Porous Air Bearings." (2005).
- [9] Luong, TS *et al* "Numerical and experimental analysis of aerostatic thrust bearings with porous restrictors." Tribology International 37, no. 10 (2004): 825-832.
- [10] Goodwin, EP, and Wyant JC, "Field Guide to Interferometric Optical Testing." SPIE, 2006: https://spie.org/publications/fg10_p24-25_zernike-polynomials.